Dear author,

Please note that changes made in the online proofing system will be added to the article before publication but are not reflected in this PDF.

We also ask that this file not be used for submitting corrections.

Mechanism and Machine Theory xxx (2018) xxx–xxx

Contents lists available at ScienceDirect

Mechanism and Machine Theory

journal homepage: www.elsevier.com/locate/mechmachtheory

ELSEVIER

Research paper

Composed continuum mechanism for compliant mechanical postural synergy: An anthropomorphic hand design example

Q1 Kai Xu [a,*], Zenghui Liu [b], Bin Zhao [b], Huan Liu [b], Xiangyang Zhu [a]

[a] State Key Laboratory of Mechanical System and Vibration, School of Mechanical Engineering, Shanghai Jiao Tong University, Shanghai 200240, China
[b] UM-SJTU Joint Institute, Shanghai Jiao Tong University, Shanghai 200240, China

ARTICLE INFO

Article history:
Received 12 April 2018
Revised 6 July 2018
Accepted 16 August 2018
Available online xxx

Keywords:
Anthropomorphic hand
Comps hand
Continuum mechanism
Grasp
Postural synergy

ABSTRACT

Continuum mechanisms have recently been used in various manipulator designs, often for medical applications. Instead of forming manipulators, a multi-backbone continuum mechanism, in a composed configuration, can be alternatively used as a transmission unit to generate an arbitrary number of translating outputs that are linearly combined from two independent inputs. This CCM (Composed Continuum Mechanism), applicable in other design scenarios, is applied as mechanical postural synergies of an anthropomorphic robotic hand. In this hand, three actuators actuate the CCM in its coordinated motion mode to drive the eleven hand joints according to two synergy inputs to form synergy-based hand poses in a pre-grasp phase. Then, the CCM closes the fingers in its synchronized motion mode. Joint-level compliance was selectively introduced based on a statics analysis to help achieve the stable grasping and pinching of many daily life objects. The compliance calculation, postural synergy synthesis, system descriptions and experimental characterizations of this hand with Compliant Mechanical Postural Synergy (the CoMPS hand) are expounded. The efficacy of the hand, demonstrated by the experimental results, can inspire its use as a prosthesis, as a training device for synergy control, or in a humanoid robot, showing the potentials of the proposed CCM.

1. Introduction

A continuum robot, a term coined in [1], often possesses a structure with one or more continuum mechanisms. A continuum mechanism, which has no identifiable revolute joints, realizes motions and transmits forces by its structural deformation. Enabled by recent advances in mechanics and kinematics modeling [2], continuum mechanisms have been used in various manipulator designs to achieve design compactness and motion dexterity, often for medical applications [3-6].

Instead of forming manipulators or catheter tips, continuum mechanisms with multiple backbones, in a composed configuration, can be alternatively used as a transmission unit to generate an arbitrary number of translating outputs that are linearly combined from two independent inputs. The working principle of the CCM (Composed Continuum Mechanism) is detailed in Section 2. The CCM, applicable in other design scenarios, can be applied as the mechanical postural synergies of an anthropomorphic robotic hand.

Q2 * Corresponding author.
E-mail address: k.xu@sjtu.edu.cn (K. Xu).

https://doi.org/10.1016/j.mechmachtheory.2018.08.015
0094-114X/

Please cite this article as: K. Xu et al., Composed continuum mechanism for compliant mechanical postural synergy: An anthropomorphic hand design example, Mechanism and Machine Theory (2018), https://doi.org/10.1016/j.mechmachtheory.2018.08.015

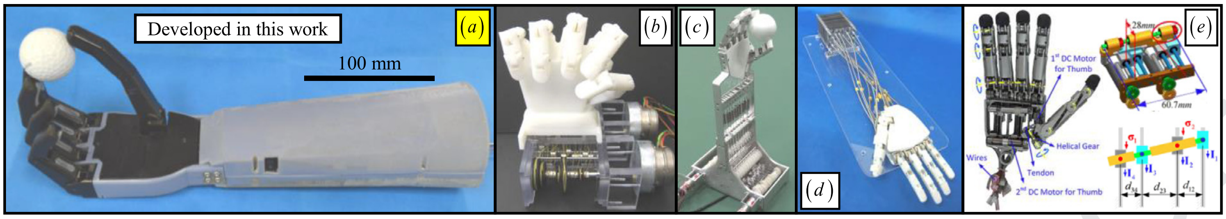

Fig. 1. Robotic hands with mechanical synergies: (a) the CoMPS hand: (b) and (c) the hands using differential pulleys in [25,27], (d) the hand using planetary gears from [18], and the X-hand using linkages in [28].

A postural synergy originally refers to a coordinated contraction pattern of a group of muscles [7]. The use of only two primary postural synergies was shown to account for a majority (approximately 84%) of the variance in many daily life grasps [8], enabling low dimensional control of a multi-joint hand.

The postural synergies (or the EigenGrasps in [9]) have triggered new developments in theories and applications. Now, even a low-bandwidth bio-signal interface (e.g., electro-myography) can control a multi-joint hand for dexterous grasps. This postural synergy provides new understanding into hand motion atlas that used to primarily consist of discrete grasp taxonomy as in [10-12]. It also has enabled new approaches for grasp planning and in-hand manipulation [13-18].

If implemented according to the linear algebra definition, postural synergies are referred to as hard synergies [19]. The synergy-level compliance [20], the joint-level compliance (namely, soft synergy as in [14]), and the synergy-level adaption (namely, adaptive synergy as in [19]) have been proposed to achieve adaptive grasps.

Postural synergies can be implemented mechanically or digitally. For example, two to three postural synergies were digitally implemented in controllers used to control 12–24 motors in a hand in [15,20-24]. The use of multiple motors and digital synergies is beneficial for forming versatile grasps and incorporating joint-level or synergy-level compliance. However, this type of hand can be complex and expensive to produce.

Transmission units, serving as mechanical postural synergies, generate multiple outputs by linearly combining two motion inputs. The mechanical synergies are realized using differential pulleys [25-27], planetary gears [18] and linkages [28] as shown in Fig. 1(b)–(e).

Efforts to find alternative designs for mechanical synergies with better design compactness led to the proposal of the CCM's first use in [29]. This paper presents the continued developments for this redesigned anthropomorphic hand with Compliant Mechanical Postural Synergies (the CoMPS hand) as shown in Fig. 1(a).

The contributions of this continued development include the following three aspects:

- The CCM is used in two motion modes. In the coordinated motion mode, the CCM is driven to form synergy-based hand poses in a pre-grasp phase. In the synchronized motion mode, the CCM is driven to close the fingers. Only the first mode is used in [29], whereas other mechanical synergy designs in [18,25-28] may require additional structure components to realize simultaneous finger closing.
- Joint-level compliance is selectively introduced based on a statics analysis, particularly for achieving stable[1] pinching motions. Grasps are easier to produce due to the form closure. Although similar ideas of soft synergies are proposed in [14,17], this study extends their validity: (i) the effectiveness of the joint-level compliance for pinching is experimentally verified; (ii) the statics analysis used for the compliance calculation for the pinching motion considers finger linkage; and (iii) closing the fingers with more force can now generate a larger pinch force to stably pinch a heavier object, instead of incurring a pinch ejection as observed in [30].
- The mechatronics and structural designs of the CoMPS hand are completely redone from those in [29]. Comprehensive experimental characterizations were performed to fully demonstrate the hand's features.

In addition to the abovementioned contributions, this paper expands the functionality of continuum mechanisms at a higher level, beyond the widely known uses as manipulator bodies or catheter tips. Here, the CCM generates linearly combined outputs. In a related study [31], another motion transmission mechanism, the continuum differential mechanism, was proposed to generate differential outputs by structural deformations. Existing differential mechanisms rely on the relative motions of their kinematic pairs for outputs.

The CoMPS hand can be applied in a humanoid robot, as prosthesis, or as an amputee training device for synergy-based control. In the latter case, an amputee can learn how to drive the synergy-based hand to form hand poses in the pre-grasp phase and simply close the fingers to produce stable grasps and pinches, possibly using the inputs decoded from his/her EMG signals following the approaches in [32,33]. Furthermore, the presented sensitivity studies indicate how accurate an amputee shall reproduce the pre-grasp poses to achieve stable grasps and pinches, providing a quantitative learning goal. Training with the use of an actual CoMPS hand can provide a better perception than with the use of a simulation (e.g., in [33]). Actual training for such amputees may be included in a future study.

[1] Stability of a grasp or a pinch in this study is defined as a static equilibrium of the hand holding an object under gravity with no other external disturbances.

Please cite this article as: K. Xu et al., Composed continuum mechanism for compliant mechanical postural synergy: An anthropomorphic hand design example, Mechanism and Machine Theory (2018), https://doi.org/10.1016/j.mechmachtheory.2018.08.015

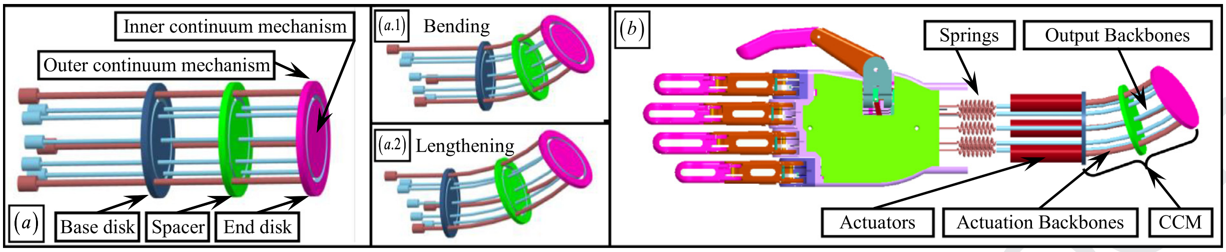

Fig. 2. The CCM: (a) the schematic with (a.1) for the coordinated motion and (a.2) for the synchronized motion, (b) its use in the CoMPS hand.

This paper is organized as follows. The design concept and overview is presented in Section 2. Section 3 describes the hand structure and the statics analysis of a pinch pose for the calculation of the joint-level compliance. The synthesis and mechanical implementations of the postural synergies are described in Section 4. Section 5 details the system components of the CoMPS hand, and Section 6 presents the experimentation. The conclusions are summarized in Section 7.

2. Design concept and overview

A CCM can generate an arbitrary number of translating outputs that are linearly combined from two independent inputs. Its use is demonstrated by the constructed CoMPS hand.

As shown in Fig. 2, a CCM consists of an outer and an inner continuum mechanism. Each continuum mechanism consists of an end disk, one or more spacers, a base disk, and several backbones (at least three for the outer continuum mechanism and an arbitrary number for the inner continuum mechanism). The backbones are made of thin nitinol rods and are attached to the end disks. They can slide with respect to the spacers and the base disks.

The CCM has three DoFs (Degrees of Freedom): two DoFs for bending and one DoF for shortening/lengthening. Then two motion modes of the CCM are utilized.

In the coordinated motion mode for the 2-DoF bending shown in Fig. 2(a.1), the three backbones of the outer mechanism are pulled and pushed to bend the outer mechanism, according to two configuration variables (θ and δ, referred to in Section 4.2). Next, the outer mechanism bends the inner mechanism. Because of the mechanism's backdrivability, all the backbones of the inner mechanism generate translating outputs that are equal to the linear combinations of the two independent inputs.

In the synchronized motion mode as in Fig. 2(a.2), the three outer backbones are simultaneously pulled or pushed to shorten or lengthen the outer mechanism together with the inner mechanism, generating the same translations for the inner backbones. The CCM's working principle is also shown in the multimedia extension.

When the CCM is implemented in the CoMPS hand as in Fig. 2(b), the three outer backbones are attached to three actuators for actuation. The finger joints are driven by the outputs from the backbones of the inner mechanism, where springs are serially connected to introduce compliance. The spring stiffness is determined using the analysis described in Section 3.2.

In the coordinated motion mode, the translating outputs of the CCM depend on two variables (θ and δ), even though the CCM is bent by three actuators. This is equivalent to combining two postural synergies to form hand poses in a pre-grasp phase. When the CCM is lengthened in the synchronized motion mode, it is equivalent to pulling all the output backbones together to close the fingers.

The hand has 11 joints: three for the thumb and two for each finger. The T, I, M, R and L letters indicate the thumb, the index finger, the middle finger, the ring finger and the little finger, respectively. The abbreviations *rot*, *mcp*, *ip*, *abd*, *pip* and *dip* indicate the rotation, the metacarpophalangeal, the interphalangeal, the abduction, the proximal and the distal interphalangeal joints, respectively. The T_{ip} joint and the *dip* joints of the fingers are fixed to simplify the hand structure.

The CCM can generate an arbitrary number of outputs by placing corresponding output backbones in the inner continuum mechanism. The arrangement of an output backbone determines the coefficients for the linear combination, referred to in Section 4.3. On the contrary, one additional set of pulleys or gears is always required for an additional output in these existing designs [18,25-27].

3. Hand design description and analysis

Designs of the fingers and the thumb are presented in Section 3.1. Section 3.2 introduces the statics analysis for determining the joint-level compliance to achieve stable pinches.

Please cite this article as: K. Xu et al., Composed continuum mechanism for compliant mechanical postural synergy: An anthropomorphic hand design example, Mechanism and Machine Theory (2018), https://doi.org/10.1016/j.mechmachtheory.2018.08.015

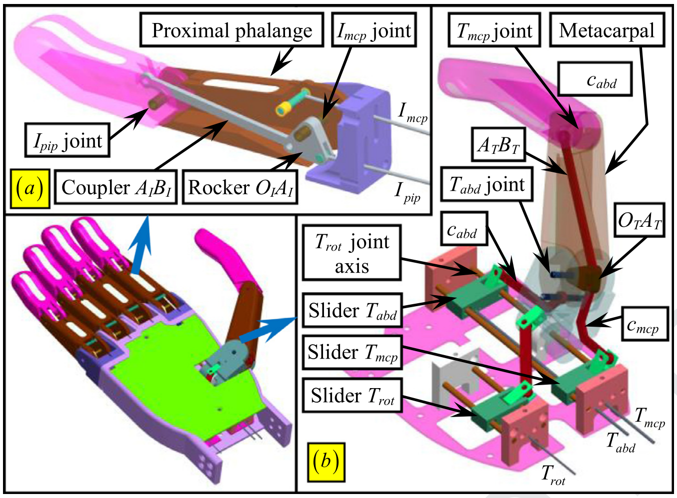

Fig. 3. The CoMPS hand: (a) the index finger, and (b) the thumb.

Table 1
Structural parameters of the CoMPS hand (Unit: mm).

	Thumb	Index	Middle	Ring	Little
Distal phalange	27	20	21	21	20
Intermediate phalange	–	25	28	27	21
Proximal phalange	32	47	48	46	40
Metacarpal	46	–	–	–	–
$\|O_XA_X\|$†	7.4	7.5	7.7	7.4	6.4
$\|A_XB_X\|$†	44.6	45.6	46.6	44.6	38.8
$\|B_XC_X\|$†	6.0	6.1	6.2	6.0	5.2

† The subscript X represents T, I, M, R or L for the five fingers, respectively.

3.1. Design descriptions of the fingers and the thumb

The design of the CoMPS hand is shown in Fig. 3. The phalange lengths were set according to the studies on hand anatomy [34,35], with the goal of achieving stable tripod pinches. All the phalange lengths, which are rounded to millimeters, are listed in Table 1.

As explained in Section 2, the CCM's translational outputs are used to drive the CoMPS hand. Hence, the actuation scheme of the thumb and the fingers solely uses pulling and pushing actions.

Because the finger designs are similar for all fingers, only the index finger is depicted in Fig. 3(a). The I_{mcp} joint is actuated by pulling or pushing the I_{mcp} rod. Pulling or pushing the I_{pip} rod actuates the I_{pip} joint through coupler A_IB_I and rocker O_IA_I. As indicated in Fig. 4, the distance between the I_{pip} joint (the C_I point) and the connection point B_I is B_IC_I. The link lengths were set proportionally according to the design of the Vincent hand in [36], as listed in Table 1. The I_{dip} joint was fixed to 20° to simplify the finger actuation.

The actuation scheme of the thumb is shown in Fig. 3(b). The T_{rot} slider is translated by pushing or pulling the T_{rot} rod. A coupler connects the thumb to the T_{rot} slider so that translation of the T_{rot} slider rotates the thumb (e.g., forms opposition). The T_{abd} and T_{mcp} joints are actuated by the couplers c_{abd} and c_{mcp}, respectively. The two couplers also rotate about the T_{rot} joint axis together with the thumb. The c_{mcp} coupler is connected to the coupler A_TB_T through the rocker O_TA_T to drive the T_{mcp} joint. As indicated in Fig. 4, the distance between the T_{mcp} joint (the C_T point) and the connection point B_T is B_TC_T. The link lengths are listed in Table 1. The T_{ip} joint was fixed to 20° to simplify the thumb actuation.

The geometrical parameters of the fingers (e.g., the angles between the various links) were all set according to the Vincent hand in [36]. All the actuation rods for the hand joints (the joint driving rods) are made of super-elastic nitinol with a diameter of 0.7 mm. The rods can be both pulled and pushed.

3.2. Statics analysis for joint compliance

After the CoMPS hand is driven to form a pre-grasp pose using the two synergy inputs, a stable pinch is considered to be relatively difficult to achieve while closing all the fingers (stable grasps are easier due to the form closure). Therefore, more attention is focused on the statics analysis of a pinch pose, schematically shown in Fig. 4.

Please cite this article as: K. Xu et al., Composed continuum mechanism for compliant mechanical postural synergy: An anthropomorphic hand design example, Mechanism and Machine Theory (2018), https://doi.org/10.1016/j.mechmachtheory.2018.08.015

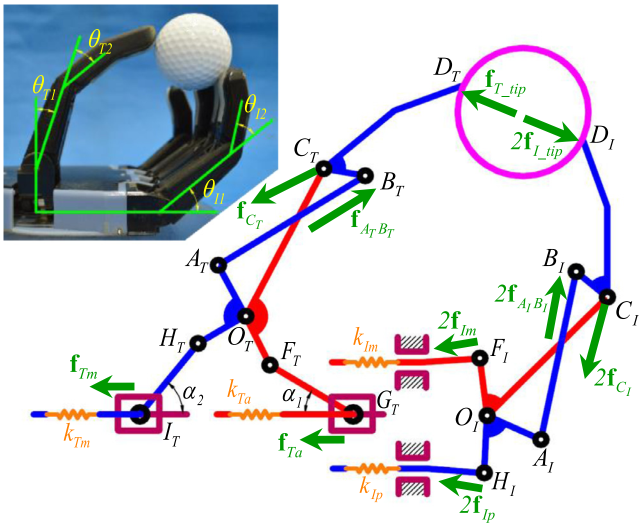

Fig. 4. Schematic of the statics analysis of a pinch pose.

This statics analysis is necessary to properly determine the joint-level compliance in the CoMPS hand. If the compliance is improperly set, closing the fingers more forcefully can lead to a pinch ejection as observed in [30], instead of generating larger pinch forces required to stably grip a heavier object.

For simplicity, the middle finger is assumed to be identical to the index finger and the T_{rot} joint rotates 90° In this way, the tripod pinch becomes a planar pinch.

As for the index finger, the moment equilibrium of the links $F_IO_IC_I$ and $H_IO_IA_I$ are given as (1) and (2), respectively. The coefficient of 2 indicates the two identical forces from the index finger and the middle finger. The force and moment equilibrium of the link $B_IC_ID_I$ is given by (3) and (4), respectively.

$$\overrightarrow{O_IF_I} \times 2\mathbf{f}_{Im} + \overrightarrow{O_IC_I} \times 2\mathbf{f}_{C_I} = \mathbf{0} \tag{1}$$

$$\overrightarrow{O_IH_I} \times 2\mathbf{f}_{Ip} + \overrightarrow{O_IA_I} \times 2\mathbf{f}_{A_IB_I} = \mathbf{0} \tag{2}$$

Where $\mathbf{f}_{Im}$ and $\mathbf{f}_{Ip}$ are the actuation forces on the nitinol rods for the I_{mcp} and I_{pip} joints; $\mathbf{f}_{A_IB_I}$ is the force exerted on the link $H_IO_IA_I$ by the link A_IB_I and $\mathbf{f}_{C_I}$ is the force exerted on the link $F_IO_IC_I$ by the link $B_IC_ID_I$.

$$(-2f_{C_I}) + \left(-2f_{A_IB_I}\right) + 2f_{I\_tip} = 0 \tag{3}$$

$$\overrightarrow{C_IB_I} \times \left(-2f_{A_IB_I}\right) + \overrightarrow{C_ID_I} \times 2f_{I\_tip} = 0 \tag{4}$$

Similarly, for the thumb, the moment equilibrium of the links $F_TO_TC_T$ and $H_TO_TA_T$ is given by (5) and (6), whereas the force and moment equilibrium of the link $B_TC_TD_T$ is given by (7) and (8), respectively.

$$\overrightarrow{O_TF_T} \times \left(\frac{\| f_{Ta} \|}{\cos\alpha_1} \cdot \frac{\overrightarrow{G_TF_T}}{\left\| \overrightarrow{G_TF_T} \right\|} \right) + \overrightarrow{O_TC_T} \times f_{C_T} = 0 \tag{5}$$

$$\overrightarrow{O_TH_T} \times \left(\frac{\| f_{Tm} \|}{\cos\alpha_2} \cdot \frac{\overrightarrow{I_TH_T}}{\left\| \overrightarrow{I_TH_T} \right\|} \right) + \overrightarrow{O_TA_T} \times f_{A_TB_T} = 0 \tag{6}$$

Where $\mathbf{f}_{Ta}$ and $\mathbf{f}_{Tm}$ are the actuation forces on the nitinol rods for the T_{abd} and T_{mcp} joints, respectively; $\mathbf{f}_{A_TB_T}$ is the force exerted on the link $H_TO_TA_T$ by the link A_TB_T and $\mathbf{f}_{C_T}$ is the force exerted on the link $F_TO_TC_T$ by the link $B_TC_TD_T$.

$$(-\mathbf{f}_{C_T}) + (-\mathbf{f}_{A_TB_T}) + \mathbf{f}_{T\_tip} = 0 \tag{7}$$

$$\overrightarrow{C_TB_T} \times (-\mathbf{f}_{A_TB_T}) + \overrightarrow{C_TD_T} \times \mathbf{f}_{T\_tip} = 0 \tag{8}$$

It is important to note that an infinite number of tripod pinches can be achieved with the independent actuation of the involved joints (namely, the T_{rot}, T_{abd}, T_{mcp}, I_{mcp}, I_{pip}, M_{mcp} and M_{pip} joints). One motivation for this development is to

Please cite this article as: K. Xu et al., Composed continuum mechanism for compliant mechanical postural synergy: An anthropomorphic hand design example, Mechanism and Machine Theory (2018), https://doi.org/10.1016/j.mechmachtheory.2018.08.015

Table 2
Determination of the joint compliance.

Joint	T_{abd}	T_{mcp}	I_{mcp}	I_{pip}
Joint driving force (N)	$\|\|\mathbf{f}_{Ta}\|\| = 21.4$	$\|\|\mathbf{f}_{Tm}\|\| = 5.2$	$\|\|\mathbf{f}_{Im}\|\| = 9.6$	$\|\|\mathbf{f}_{Ip}\|\| = 3.9$
Desired total stiffness (N/mm)	93.5	22.7	41.9	17.0
Nitinol rod stiffness (N/mm)	93.5	93.5	74.8	74.8
Desired spring stiffness (N/mm)	∞	30.0	95.5	22.1
Adopted spring stiffness (N/mm)	∞	**30**	**90**	**30**

demonstrate that a synergy-based anthropomorphic hand can produce stable grasps and pinches. The task is considered accomplished even when only one pinch is stably reproduced. For this reason, the statics analysis was performed for the specific pose that was formed manually as shown in the inset of Fig. 4. This pose was also used in the synergy synthesis presented in Section 4.1.

Under this particular pinch pose in Fig. 4, various actuation forces might all lead to the pose stability considering different contact conditions between the pinched ball and the fingers. However, only one set of the joint compliance needs to be determined. A point contact without friction was assumed for simplification. In reality, friction will always exist and can actually improve the pinch stability. This assumption is validated by the wide range of synergy inputs that can achieve stable pinching, which are described in the sensitivity study in Section 6.2.

As shown in Fig. 2(b), springs with different stiffness are serially integrated into the joint-driving rods for joint compliance. When the CoMPS hand is commanded to gradually close its fingers under the lengthening actuation of the CCM, it is equivalent to applying different actuation forces to the joints.

Joint angles for the T_{abd} (θ_{T1}), T_{mcp} (θ_{T2}), I_{mcp} (θ_{I1}) and I_{pip} (θ_{I2}) joints were measured from the actual pinch pose shown in Fig. 4. The pinch forces ($\mathbf{f}_{T\_tip}$ and $\mathbf{f}_{I\_tip}$) should pass through the center of the ball to avoid ejection. $||\mathbf{f}_{T\_tip}||$ is assumed to be 1 N whereas $||\mathbf{f}_{I\_tip}||$ is assumed to be 0.5 N (the middle finger generates the other 0.5 N pinch force to maintain the equilibrium). Such unit pinch forces are assumed because only the ratios between the joint actuation forces are of interest.

With the structural parameters listed in Table 1, the joint angles measured and the pinch forces assumed, the joint driving forces on the nitinol rods for the T_{abd}, T_{mcp}, I_{mcp} and I_{pip} joints can be obtained using (1) to (8) as listed in the 2nd row of Table 2. Next, the ratios between the desired total stiffness (including the stiffness from the spring and the nitinol rod) for each joint should be proportional to the corresponding driving forces.

The nitinol rod for driving the hand joint has limited stiffness that can be calculated as $k = EA \,/\, l$ (E for the Young's modulus, A for the cross-sectional area and l for the rod length). The stiffness of the driving rods is listed in the 4th row of Table 2.

Because the T_{abd} joint has the highest driving force (21.4 N), the joint stiffness should not be further lowered. Therefore, no spring was integrated and the desired spring stiffness is listed as ∞ in Table 2. The desired total stiffness of the T_{abd} joint is the same as the nitinol rod stiffness (93.5 N/mm). According to the ratios between the joint driving forces, the desired total stiffness of the T_{mcp}, I_{mcp} and I_{pip} joints are obtained as listed in the 3rd row of Table 2. Then, the desired spring stiffness can be obtained considering the serial connection of the spring and the nitinol rod. The adopted spring stiffness is listed in the last row of Table 2, considering the availability of the springs in stock. The spring stiffness for the *mcp* and *pip* joints for the middle, the ring and the little fingers are set to the same because the ring and the little fingers are less dominant during a pinching motion.

4. Mechanical postural synergy

This paper uses the CCM to mechanically implement the postural synergy. The collection of hand poses and synergy extraction are presented in Section 4.1. The kinematics of the CCM is presented in Section 4.2 and the structural parameters are determined according to the synthesized synergy values as presented in Section 4.3.

4.1. Pose collection and postural synergy extraction

In a previous study where an in-hand manipulation of two rotating balls was realized for a synergy-based hand [18], it was found highly effective to synthesize the postural synergies directly from the poses of the to-be-controlled hand. This approach can reduce possible uncertainties and errors while translating synergies from one hand kinematics to another [37].

Postural synergies are usually extracted as the first of a few (usually two) principal components from a matrix that consists of recorded joint angles of a hand under various poses. Here, the hand pose matrix alternatively consists of the push-pull lengths of the joint driving rods because the translating outputs from the CCM are required to drive the CoMPS hand. In this way, the non-linearity between the push-pull actuation length and the hand joint angle does not complicate the synergy synthesis.

As shown in Fig. 5, eleven micrometers were manually driven to push or pull the joint driving rods to drive the eleven joints of the CoMPS hand for various grasps and pinches. The springs, whose stiffness was determined as presented in Section 3.3, were serially integrated.

Please cite this article as: K. Xu et al., Composed continuum mechanism for compliant mechanical postural synergy: An anthropomorphic hand design example, Mechanism and Machine Theory (2018), https://doi.org/10.1016/j.mechmachtheory.2018.08.015

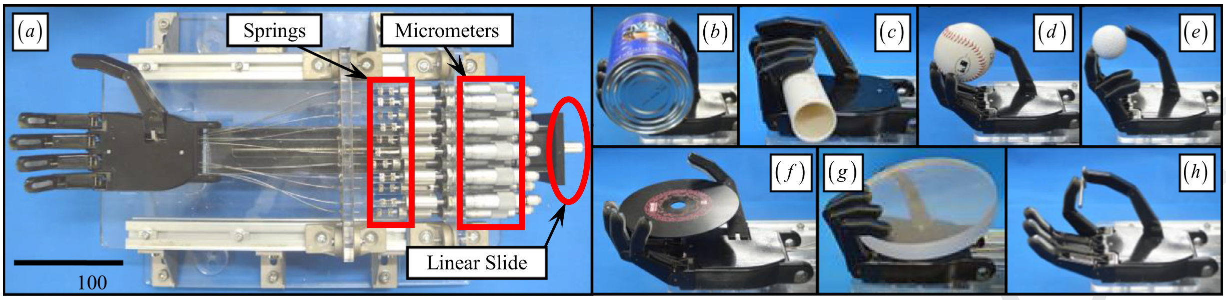

Fig. 5. Hand poses: (a) experimental setup, (b) pose #1, (c) pose #2, (d) pose #10, (e) pose #11, (f) pose #9, (g) pose #21, (h) pose #16.

The CoMPS hand poses were adopted according to the comprehensive taxonomy proposed by Feix et al. [11]. The original set includes 33 poses, covering a majority of ADL (Activities of Daily Living) hand poses. Due to the limitations on the number of joints (e.g., no finger abduction in the CoMPS hand) and the joint motion ranges, several poses could not be reproduced, such as those for holding scissors, holding chopsticks, and the abduction grip between the fingers.

In addition to utilizing the 2-DoF bending of the CCM to produce the linear combination of two postural synergies, the CoMPS hands utilizes the 1-DoF lengthening of the CCM to close all fingers. To replicate the finger closing motion, all the micrometers were placed on a linear slide to pull the joint driving rods together, as in Fig. 5(a).

The pose was considered valid only when stable grasping or pinching was achieved by actuating the linear slide to close all of the fingers. With the serially integrated springs with different stiffness, different driving forces were applied to the joints. Although the spring stiffness was determined according to the statics analysis for one pinch pose, the CoMPS hand was able to perform many stable grasps because a stable grasp is easier to achieve under the enveloping motions of the palm and all of the fingers.

Twenty three grasps and pinches from the GRASP taxonomy [11] were reproduced. The seven representative poses are: pose #1 for grasping a large can, pose #2 for grasping a round bar, pose #10 for pinching a baseball, pose #11 for tripod pinching a golf ball, pose #9 for precision grasp of a CD, pose #21 for the palmar grasp of a thick disk, and pose #16 for tip pinch of a thin stick, shown in Fig. 5(b)–(h), respectively. This particular listing sequence is for better comparison with the pose reproduction experiments described in Section 6.1.

For the pinching poses, the fingers were first actuated to only balance the gravitational force on the pinched objects. Then, the linear slide was actuated for 2 mm to gradually close the fingers. For all 23 poses, the stability of the grasps and pinches was maintained. The poses were adjusted if they could not maintain the stability during the finger closing motion.

The measured rod driving lengths of each joint for the 23 poses are not listed explicitly for brevity. A zero actuation length corresponds to a fully extended hand pose.

Each of the 23 hand poses can be expressed as a pose vector $\mathbf{p}_j \in \Re^{11\times 1}$ ($j = 1, 2,..., 23$), whose elements are the corresponding joint driving lengths. The 23 pose vectors can be arranged to form a pose matrix $\mathbf{P}$. Singular value decomposition can be performed on $\mathbf{P}$ as in (9).

$$\mathbf{P}_{11\times 23} = \begin{bmatrix} \mathbf{p}_1 & \mathbf{p}_2 & \cdots & \mathbf{p}_{23} \end{bmatrix} = \bar{\mathbf{P}}_{11\times 23} + \mathbf{U}_{11\times 11}\mathbf{\Sigma}_{11\times 23}\mathbf{V}^T_{23\times 23} \tag{9}$$

Where $\bar{\mathbf{P}} = [\ \bar{\mathbf{p}} \quad \bar{\mathbf{p}} \quad \cdots \quad \bar{\mathbf{p}}\ ]$ with $\bar{\mathbf{p}} = \frac{1}{23}\sum_{j=1}^{23}\mathbf{p}_j$ is the average pose matrix.

Keeping the two largest singular values in $\mathbf{\Sigma}$ (namely, setting the rest of the singular values to zero) in (9) gives (10).

$$\mathbf{P} \approx \tilde{\mathbf{P}} = \bar{\mathbf{P}} + \begin{bmatrix} \mathbf{u}_1 & \mathbf{u}_2 \end{bmatrix}\begin{bmatrix} g_{1\,1} & g_{1\,2} & \cdots & g_{1\,23} \\ g_{2\,1} & g_{2\,2} & \cdots & g_{2\,23} \end{bmatrix} \tag{10}$$

Then, each pose is approximated as in (11).

$$\mathbf{p}_j \approx \tilde{\mathbf{p}}_j = \bar{\mathbf{p}} + g_{1j}\mathbf{u}_1 + g_{2j}\mathbf{u}_2,\ j = 1, 2, \ldots, 23 \tag{11}$$

Where $\mathbf{u}_1$ and $\mathbf{u}_2$ are referred to as the postural synergies. These postural synergies can be directly used to determine the structural parameters of the CCM as presented in Section 4.3.

Any hand pose can be approximated as in (12), applying the average hand pose $\bar{\mathbf{p}}$, the hand driving vector $\Delta\mathbf{p}$ and two synergy inputs g_1 and g_2.

$$\mathbf{p} \approx \bar{\mathbf{p}} + \Delta\mathbf{p} \text{ and } \Delta\mathbf{p} = g_1\mathbf{u}_1 + g_2\mathbf{u}_2 \tag{12}$$

4.2. Kinematics of the composed continuum mechanism

The CCM in Fig. 6 is used to mechanically implement the postural synergies. It has three actuation backbones and eleven output backbones. The attached disks and spacers shown in Fig. 2(a) were built as one piece. A central virtual backbone

Please cite this article as: K. Xu et al., Composed continuum mechanism for compliant mechanical postural synergy: An anthropomorphic hand design example, Mechanism and Machine Theory (2018), https://doi.org/10.1016/j.mechmachtheory.2018.08.015

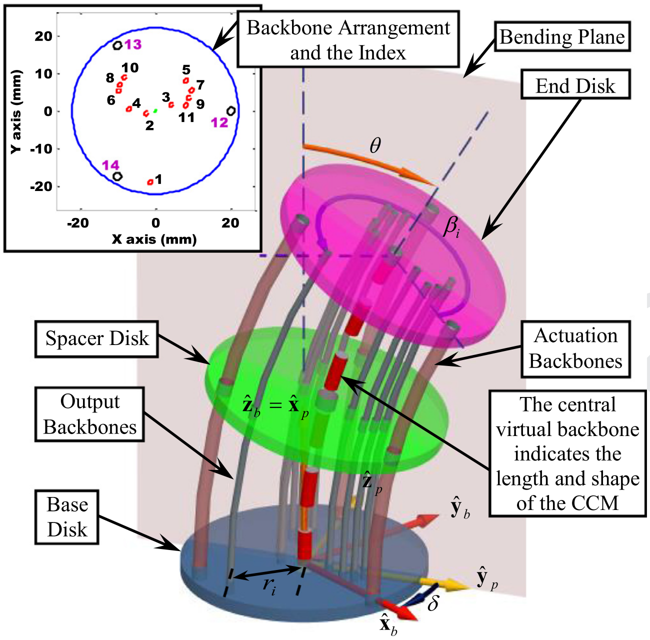

Fig. 6. Nomenclature and coordinates of the CCM with the arrangement of the backbones shown in the inset: 1 to 11 for outputs and 12 to 14 for actuation.

characterizes the length and bending shape of the CCM. The actuation backbones and the output backbones are all made of thin super-elastic nitinol rods.

The push-pull actuation of the actuation backbones bends the CCM, leading to translational outputs of the output backbones. Two coordinate systems are defined as follows, while the nomenclature is defined in Table 4.

- ➢ *Base Disk Coordinate System* (BDS) is designated as $\{b\} \equiv \{\hat{\mathbf{x}}_b, \hat{\mathbf{y}}_b, \hat{\mathbf{z}}_b\}$. Its XY plane coincides with the base disk of the CCM and its origin is at the center.
- ➢ *Bending Plane Coordinate System* (BPS) is designated as $\{p\} \equiv \{\hat{\mathbf{x}}_p, \hat{\mathbf{y}}_p, \hat{\mathbf{z}}_p\}$ which shares its origin with $\{b\}$ and has the CCM's virtual backbone bending in its XY plane.

Kinematics modeling of the CCM adopts a widely accepted assumption that the bent shape, which is characterized by the central virtual backbone, is circular. This assumption has previously been analytically and experimentally verified [38,39]. Under this assumption, the backbones all bend into circular arcs in planes parallel to the bending plane.

With detailed derivations available in the previous studies [31,38,39], the length of the ith backbone l_i satisfies (13), whereas q_i is then written as (14). Please note that when the CCM is bent towards one backbone, its length l_i within the CCM is shortened, generating a pushing output. This "pushing" output is negative in view of the hand joint due to the definition of the joint driving length. Hence, the definition of q_i has been kept harmonic with the sign of the joint driving lengths in the hand pose vector $\mathbf{p}_j$. This means that the q_i value from (14) directly matches the corresponding joint driving length.

$$l_o = l_i + r_i\theta \cos(\delta + \beta_i) \tag{13}$$

$$q_i = -r_i\theta \cos(\delta + \beta_i) \tag{14}$$

4.3. Structural determination of the synthesized synergies

When the CCM is bent, (14) holds for all the backbones. The backbone's arrangement is indicated by the corresponding r_i and β_i values. Because the 11 output backbones (i = 1, 2, …, 11) drive the CoMPS hand from the average pose $\bar{\mathbf{p}}$, these outputs, the q_i in (14), can be put together to form the hand driving vector $\Delta\mathbf{p}$ in (15).

$$\Delta\mathbf{p} = \begin{bmatrix} -r_1\theta\cos(\delta+\beta_1) & -r_2\theta\cos(\delta+\beta_2) & \ldots & -r_{11}\theta\cos(\delta+\beta_{11}) \end{bmatrix}^T \tag{15}$$

Expanding $\cos(\delta + \beta_i)$ in (15) gives (16), where r_{ref} is used to normalize the expression. Please note that r_i and β_i are constant for a built CCM.

Comparing (16) with (12) indicates that a hand pose $\mathbf{p}$, which involves two synergy inputs g_1 and g_2, corresponds to a pair of θ and δ values. In other words, each configuration of the CCM (specified by θ and δ) determines a hand pose. The

Please cite this article as: K. Xu et al., Composed continuum mechanism for compliant mechanical postural synergy: An anthropomorphic hand design example, Mechanism and Machine Theory (2018), https://doi.org/10.1016/j.mechmachtheory.2018.08.015

Table 3
Niti rod actuation lengths (unit: millimeter).

	T_{rot}	T_{abd}	T_{mcp}	I_{mcp}	I_{pip}	M_{mcp}	M_{pip}	R_{mcp}	R_{pip}	L_{mcp}	L_{pip}
$\bar{\mathbf{p}}$	12.92	3.28	1.01	5.32	−0.42	5.74	−0.82	6.17	−1.09	7.05	−2.64
$\mathbf{u}_1$	−0.05	−0.10	0.17	−0.28	0.32	−0.39	0.38	−0.38	0.35	−0.33	0.33
$\mathbf{u}_2$	−0.76	−0.02	0.06	0.02	0.32	0.22	0.22	0.28	0.14	0.36	0.06

Table 4
Nomenclature for the kinematics of the CCM.

Symbol	Definition
i	Index of the backbones
r_i	Distance from the central backbone to the ith backbone
β_i	Division angle between the ith backbone and $\hat{x}_b$; β_i remain constant once the CCM is built.
l_i	Length of the ith backbone measured from the base disk to the end disk
l_o	Original length of the backbones when the CCM is in its initial straight configuration
q_i	Translation distance of the ith backbone; $q_i \equiv l_i - l_o$
δ_i	A right-handed rotation angle about $\hat{z}_b$ from $\hat{y}_p$ to a ray passing through the central backbone and the ith backbone.
δ	$\delta \equiv \delta_1$ and $\delta_i = \delta + \beta_i$
$\theta(s)$	The angle of the tangent to the central backbone along its length in the bending plane. This angle at the tip of the central backbone is of more interest and it is designated as ϑ.

mapping between (g_1, g_2) and (θ, δ) is expressed as (17).

$$\Delta\mathbf{p} = r_{ref}\theta \sin\delta \begin{bmatrix} \frac{r_1}{r_{ref}}\sin\beta_1 \\ \frac{r_2}{r_{ref}}\sin\beta_2 \\ \vdots \\ \frac{r_{11}}{r_{ref}}\sin\beta_{11} \end{bmatrix} + \left(-r_{ref}\theta\cos\delta\right) \begin{bmatrix} \frac{r_1}{r_{ref}}\cos\beta_1 \\ \frac{r_2}{r_{ref}}\cos\beta_2 \\ \vdots \\ \frac{r_{11}}{r_{ref}}\cos\beta_{11} \end{bmatrix} \tag{16}$$

$$\begin{cases} g_1 = r_{ref}\theta\sin\delta \\ g_2 = -r_{ref}\theta\cos\delta \end{cases} \Leftrightarrow \begin{cases} \delta = \operatorname{atan2}(g_1/\theta, -g_2/\theta) \\ \theta = \sqrt{g_1^2 + g_2^2}/r_{ref} \end{cases} \tag{17}$$

Where atan2(y, x) is the right-handed angle between the x-axis and a ray passing through the origin and the point (x, y).

Then, the elements in $\mathbf{u}_1$ and $\mathbf{u}_2$ can be used to calculate r_i and β_i as in (18) to determine the backbone arrangement.

$$\begin{cases} r_i = r_{ref}\sqrt{u_{1\_i}^2 + u_{2\_i}^2} \\ \beta_i = \operatorname{atan2}(u_{2\_i}, u_{1\_i}) \end{cases} \tag{18}$$

Where u_{1_i} and u_{2_i} are the ith element in $\mathbf{u}_1$ and $\mathbf{u}_2$, respectively.

It can be observed from (18) that the r_{ref} value scales the distribution of the output backbones. If r_{ref} is too large, it will be difficult to fit the CCM inside the CoMPS hand. If r_{ref} is too small, an excessive bending of the CCM will be required. Thus, r_{ref} is set to 25 mm. The $\mathbf{u}_1$ and $\mathbf{u}_2$ values listed in Table 3 can be used to calculate the corresponding r_i and β_i values ($i = 1, 2, \ldots, 11$). The resultant arrangement of the eleven output backbones is shown in the inset of Fig. 6.

An arbitrary pair of θ and δ values corresponds to a pair to g_1 and g_2 values and a hand pose. Three actuation backbones ($i = 12, 13, 14$) were pushed and pulled to bend the CCM into a configuration specified by θ and δ, according to (14). The r_i and β_i values are set as follows to facilitate the component arrangement, although they can be set arbitrarily: $r_{12} = r_{13} = r_{14} = 20$ mm, $\beta_{12} = 0$, $\beta_{13} = 2\pi/3$ and $\beta_{14} = 4\pi/3$.

The three actuation backbones are first pushed and pulled to bend the CCM to form a pre-grasp pose. They are then pushed together to lengthen the CCM to close all the fingers to achieve grasps and pinches.

5. Hand and controller descriptions

The CoMPS hand was assembled as shown in Fig. 7. The components include: i) the hand, ii) a controller board, iii) three servomotors with gearheads, iv) three lead screws with three potentiometers, v) a battery pack, and vi) the CCM with three actuation backbones and eleven output backbones. The output backbones are connected with the joint driving rods using serially integrated springs for joint compliance.

Bending of the CCM drives the CoMPS hand from its average pose specified by $\bar{\mathbf{p}}$ in (11) and (12), whereas lengthening of the CCM closes the fingers to form grasps and pinches. It is important to ensure that the hand is in its average pose after assembly. The average pose $\bar{\mathbf{p}}$ is obtained by actuating the joint driving rods for the specific distances as listed in the $\bar{\mathbf{p}}$ row of Table 3. Positive values indicate pulling, whereas negative values indicate pushing.

Three Maxon servomotors (DCX12L EB SL 6V with GPX12 AA 35:1 gearhead) were used to drive three IGUS lead screws (6 mm diameter and 1 mm lead) to push and pull the actuation backbones of the CCM. Three potentiometers (KTL-50L from XiYu Electronic Co., China) were used to provide position feedback.

Please cite this article as: K. Xu et al., Composed continuum mechanism for compliant mechanical postural synergy: An anthropomorphic hand design example, Mechanism and Machine Theory (2018), https://doi.org/10.1016/j.mechmachtheory.2018.08.015

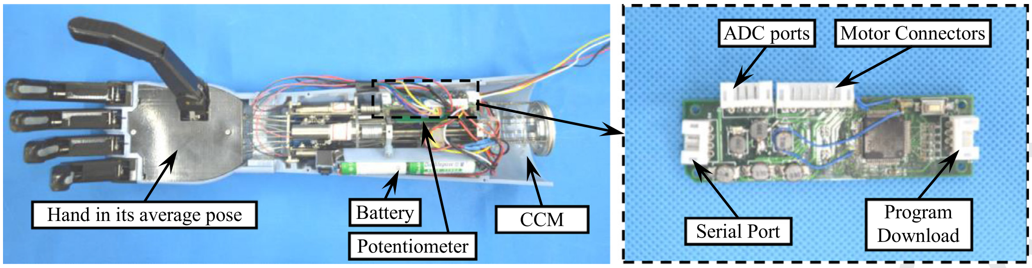

Fig. 7. The assembled CoMPS hand in its average pose.

A controller board as shown in the inset of Fig. 7 was designed and fabricated to drive the servomotors. The board was based on a STM32F415 MCU (Micro Control Unit, STMicroelectronics Co.). Two motor driver chips (DRV8833, Texas Instruments) were used to drive the three servomotors. Connectors for the ADC, serial port and program download were integrated on the board.

Two batteries of 3.7 V were connected serially for the system power supply. A voltage regulator (TPS7A6033-Q1, Texas Instruments) was used to convert the 7.4 V input into a 3.3 V output for the MCU and a 5 V output for the potentiometers.

Closed-loop PID controls at a sampling rate of 1 kHz were implemented. A moving average filter with 50 of the most recent read-outs was used as the feedback from the potentiometers to suppress noise. A position control accuracy of ± 0.05 mm was achieved.

In this study, the control commands for the CoMPS hand, including the synergy inputs (g_1 and g_2) and the finger closing length, were sent by the on-board serial port. For use as a training device for synergy control, it is possible to decode these control commands from an amputee's residual limb with several myographic electrodes. Such synergy input decoding has been attempted in [32,33].

6. Experimental characterizations

With the CoMPS hand assembled, a series of experimental characterizations were performed according to the existing studies [18,40]. The hand pose reproduction using the CCM is presented in Section 6.1. A sensitivity study is presented in Section 6.2 to demonstrate how accurate a pose must be reproduced to achieve stable tripod pinching. The quantifications of the grasp/pinch forces and the pull-out forces are presented in Sections 6.3 and 6.4, respectively.

6.1. Hand pose reproduction

The postural synergies were synthesized using 23 grasps and pinches as described in Section 4.1. A hand pose is formed using two synergy inputs (g_1 and g_2) as in (11). For each pair of synergy inputs, the CCM's configuration variables (θ and δ) are calculated according to (17). The actuation lengths of the actuation backbones are obtained using (14) such that the STM32F415 controller board drives the servomotors to push and pull the actuation backbones to bend the CCM to change the pose of the CoMPS hand.

An arbitrary pair of g_1 and g_2 may generate a hand pose that violates one or more joint limits of the CoMPS hand. Hence, an actuation zone was first established as shown in Fig. 8(a). The zone is generated by enumerating the synergy plane in increments of 0.1 mm along both the g_1 and g_2 axes. A point is admitted into the zone if the reproduced pose does not violate any joint limits. In other words, any points outside this area represent the synergy values with which the generated hand joint values using (11) violate one or more hand joint limits.

As indicated in (10), the 23 poses used for the synergy synthesis correspond to the 23 pairs of g_1 and g_2 values. In Fig. 8(a), most of the poses can be reproduced after closing the fingers a distance of 1 to 2 mm, showing the motion capability of the CoMPS hand.

As shown in Fig. 8(b.1), (c.1), (d.1), (e.1), four poses (poses #1, #2, #10 and #11 as described in Section 4.1) were reproduced using the original g_1 and g_2 values from the synergy synthesis. Then, the hand was closed by lengthening the CCM for 1.1 mm, 1.9 mm, 1.5 mm and 1.0 mm, respectively, to achieve stable grasping and pinching. The fingers were gradually closed from a distance of 1.0 mm in increments of 0.1 mm until the finger-object contacts generated enough friction to overcome the gravitational force. In Fig. 8(b.2), more actuation for closing the fingers is required, if the large can is not empty.

Comparing the pinch poses in Fig. 8(e.1) and Fig. 5(e), considerable differences can be observed because the hand pose was produced using two linear synergies. After closing the fingers for 1.0 mm, additional rotation was realized on the T_{rot} joint as the fingers were closed to achieve a stable pinch, even though the non-contacting ring and little fingers were still positioned differently.

Please cite this article as: K. Xu et al., Composed continuum mechanism for compliant mechanical postural synergy: An anthropomorphic hand design example, Mechanism and Machine Theory (2018), https://doi.org/10.1016/j.mechmachtheory.2018.08.015

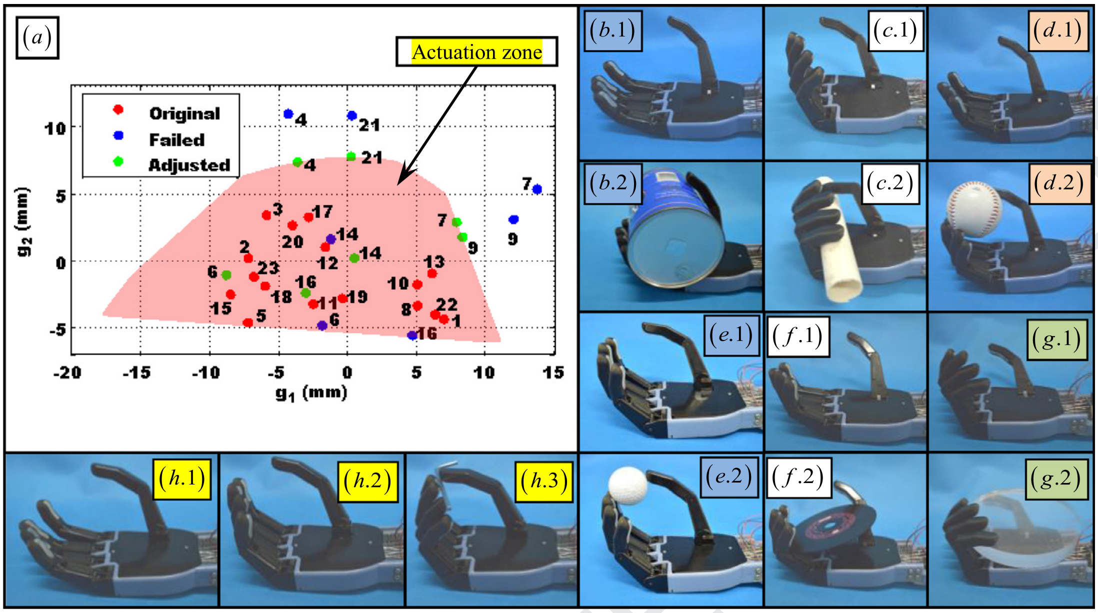

Fig. 8. Pose reproduction for grasps and pinches: (a) actuation zone, and the poses (b) #1, (c) #2, (d) #10, (e) #11, (f) #9, (g) #21, and (h) #16.

Poses #4, #7, #9 and #21 are outside the actuation zone and were reproduced via an optimization as in (19), minimizing the joint actuation errors. $\mathbf{W}_j$ is a weight matrix. It is an identity matrix for the poses outside the actuation zone.

$$\min_{g_1, g_2} \left(\mathbf{p}_j - \bar{\mathbf{p}} - g_1\mathbf{u}_1 - g_2\mathbf{u}_2\right)^T \mathbf{W}_j \left(\mathbf{p}_j - \bar{\mathbf{p}} - g_1\mathbf{u}_1 - g_2\mathbf{u}_2\right) \tag{19}$$

As shown in Fig. 8(f.1)-(g.1), poses #9 and #21 were reproduced using the adjusted g_1 and g_2 values obtained from the optimization in (19). Then, the hand was closed by lengthening the CCM for 1.5 mm and 1.0 mm to achieve precision grasping of a CD and palmar grasping of a large thick disk.

Comparing the precision grasps in Fig. 8(f.2) and Fig. 5(f), it can be observed that the precision grasp is not well reproduced. The grasped CD is constrained by the form closure created by the fingers. One fundamental reason to explain this could be that the desired g_1 and g_2 values are outside the actuation zone.

Three poses (poses #6, #14 and #16 as described in Section 4.1) were reproduced using the g_1 and g_2 values from the synergy synthesis in (10). These poses cannot fully regenerate the intended grasps/pinches, regardless of how the fingers are closed.

Using pose #16 as an example, the reproduced pose, shown in Fig. 8(h.1), is clearly different from the original pose in Fig. 5(h). The possible reason is that this is a 2-dimenional approximation of the original pose. Then, the optimization in (19) was performed to adjust the g_1 and g_2 values using a different weight matrix $\mathbf{W}_{16}$ where ones were set for the joints of the thumb and the index finger and zeros were set for the rest of the joints in the diagonal entries. This was to minimize the joint actuation errors for the fingers that are involved in the pinch. The new pair of g_1 and g_2 values were obtained and plotted as the #16 dot in green in Fig. 8(a), while the adjusted pose is shown in Fig. 8(h.2). The tip pinch was realized by lengthening the CMM for 1.5 mm, as shown in Fig. 8(h.3).

Comparing this tip pinch pose in Fig. 8(h.3) and Fig. 5(h), considerable difference can be observed in the fingers that are not originally involved in the pinch. The original tip pinch in Fig. 5(h) is reproduced with difficulty using two linear postural synergies. Because the optimization in (19) using $\mathbf{W}_{16}$ puts higher priority on the pinching fingers (the thumb and the index finger), the poses of the non-contributing fingers may be compromised.

Please note that closing the fingers under a pose near the boundaries of the actuation zone can still violate the joint actuation limits. When a joint is stopped by its mechanical limit, continuing to close the finger extends the corresponding integrated spring(s). Because the actuation for finger closing is limited to 2 mm, the hand structures are sufficiently strong to tolerate these additional actuation forces. Grasping motions of the CoMPS hand are also shown in the multimedia extension.

6.2. Sensitivity study for stable pinching

If the proposed CoMPS hand is used as a training device for synergy control, this sensitivity study, which shows how accurately the pose must be reproduced, provides a quantitative learning goal. This study also verifies the efficacy of the statics analysis for the pinching motion.

Please cite this article as: K. Xu et al., Composed continuum mechanism for compliant mechanical postural synergy: An anthropomorphic hand design example, Mechanism and Machine Theory (2018), https://doi.org/10.1016/j.mechmachtheory.2018.08.015

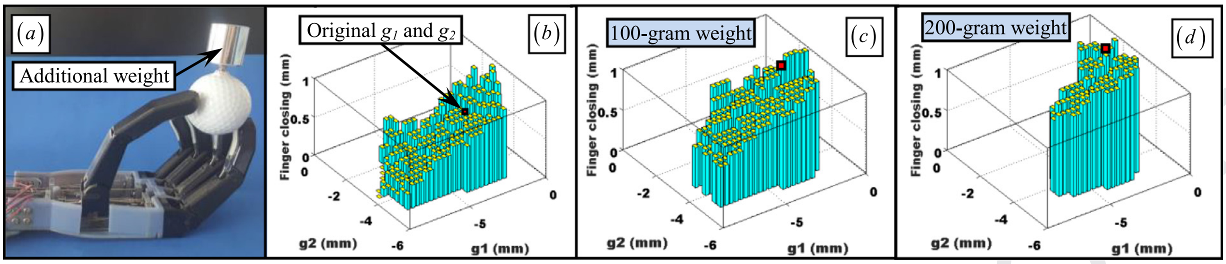

Fig. 9. Sensitivity study for the tripod pinch: (a) experimental setup, and finger closing lengths with respect to the g_1 and g_2 values for (b) a golf ball, and with (c) a 100-gram and (d) a 200-gram weight; the red block indicates the original g_1 and g_2 values from the synergy synthesis.

Because a stable pinch is more difficult to produce than a grasp, the sensitivity study is conducted for the tripod pinch in an enumerative manner. The sensitivity mentioned here means how sensitive the pinch success is to the similarity between a reproduced pose and the particular pinch pose in Fig. 4.

On the synergy plane, points around pose #11 (the tripod pinch) are tested. A point is valid if the following conditions are satisfied. A non-contacting pre-pinch pose should first be generated under the g_1 and g_2 values. Then, the golf ball is placed at a proper position by observation. This is considered acceptable. In a training session, an amputee would also actively adjust the position and orientation of the CoMPS hand to better produce grasps and pinches. Next, the fingers are gradually closed. The point is valid if the pinch can be stably achieved.

The sensitivity study is plotted in Fig. 9. To show how the sensitivity changes with respect to the weight of the pinched object, a 100-gram weight and a 200-gram weight was attached to a golf ball, as shown in Fig. 9(a).

In Fig. 9(b)–(d), the height in the Z axis represents the finger closing lengths required to achieve a stable pinch. The finger closing lengths is indicated in Fig. 2(a.2). When the composed continuum mechanism is lengthened, all the output backbones are pulled together to close the fingers. This pulling distance is the finger closing length.

While closing the fingers to achieve a pinch or grasp, the exerted forces by the fingers depend on the incorporated joint-level compliance. The joint-level compliance was determined according to the statics analysis in Section 3.2, where a point contact without friction was assumed between the fingertip and the pinched ball in sake of simplicity. In reality, friction will always exist and can actually improve the pinch stability, since the friction would occur in the opposite directions of the movement trends. It is clear from Fig. 9(b)–(d) that the CoMPS hand is capable of forming stable pinches. The pre-pinches do not need to be accurately reproduced. The validity of the statics analysis and the effectiveness of the joint-level compliance are the essential reasons for the capability of the CoMPS hand to form stable pinches even when the pre-pinches are not accurately reproduced.

When the sensitivity is low, a pose that is dissimilar to the pinch pose in Fig. 4 can still generate a stable pinch after the fingers are closed. Since the hand poses are changed by varying the g_1 and g_2 synergy values, the size of the stable pinch ranges in Fig. 9(b)–(d) indicates the level of sensitivity. In Fig. 9(d), fewer g_1 and g_2 values (around the original value indicated by the red block) can generate stable pinches. This means the sensitivity is higher for the case in Fig. 9(d).

When the g_1 and g_2 synergy values are varied to form a pre-pinch and then the fingers are closed, the exerted forces on the pinched ball may actually always deviate from the scenario in Fig. 4. The exerted pinch forces will generate friction: a portion of the friction balances the gravitational force of the pinched ball, while the rest friction balances the residual forces/moments to maintain the pinch equilibrium.

As the pinch pose and the finger forces deviate more from the analysis in Fig. 4, the residual forces/moments may also increase. Then a bigger friction is needed to balance the increased residual forces/moments. As the total available friction is bounded by the static friction coefficient, likely less friction would be available to balance the ball's gravity.

Referring to the explanations above, when a heavier ball is pinched, the finger closing lengths should first be increased to generate harder pinches. Even though, a bigger portion of the total friction may be used to balance the heavier ball's gravity. Then the rest of the friction that can balance the residual pinch forces/moments becomes limited. This demands that the pinch pose should be more similar to the pose in Fig. 4. In other words, successful pinch poses become fewer. This matches the expectation that the pre-pinch shall be reproduced more accurately to more closely resemble the pose from the pinch analysis presented in Section 3.2. This means the stable pinch range is reduced and the sensitivity increases.

When the pinch poses are similar to the one in Fig. 4, higher gripping forces can generate higher friction to balance heavier weights. When the pinch poses are dissimilar, the finger pinch forces may generate residual forces/moments that cannot be balanced by the fingertip friction. Then, the pinch failure (e.g., pinch ejection or the roll-back phenomenon observed in [30]) may occur.

6.3. Quantifications of pinching and grasping forces

It is desired that the CoMPS hand can generate sufficient grasping and pinching forces. The capabilities are quantified as follows.

Please cite this article as: K. Xu et al., Composed continuum mechanism for compliant mechanical postural synergy: An anthropomorphic hand design example, Mechanism and Machine Theory (2018), https://doi.org/10.1016/j.mechmachtheory.2018.08.015

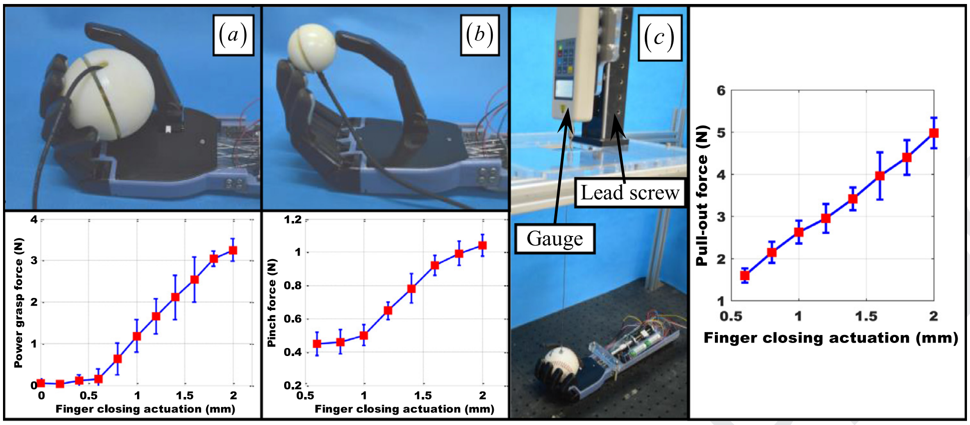

Fig. 10. Force quantifications: (a) grasp, (b) pinch, and (c) pull-out.

The grasping force quantification experiments were performed as shown in Fig. 10(a). An ATI Nano 17 force sensor was installed inside a 3D-printed ball with a diameter of 73 mm (the size of a baseball). The ball was placed between the fingers to measure the grasping force. The results are plotted in Fig. 10(a) where the finger-closing actuation increases from 0 mm to 2 mm, displaying the minimal, the average and the maximal forces when the grasp was repeated five times.

The pinching force quantification experiments were performed as shown in Fig. 10(b). The ATI Nano 17 force sensor was installed inside another 3D-printed ball with a diameter of 40 mm. The CoMPS hand was in pose #11, described in Section 6.1, and the ball was placed between the index finger, the middle finger and the thumb to produce a tripod pinch. The pinching forces were measured as the norm of the vector sum of the XYZ components from the ATI sensor, as plotted in Fig. 10(b) where the finger-closing actuation increases from 0.6 mm to 2 mm. The measurement did not start from 0 mm because a certain distance of finger-closing is required to generate sufficient friction, whereas in the grasping experiments in Fig. 10(a), the ball can rest on the palm.

The grasping and pinching forces are small, compared to the existing prosthetic devices in [36]. The reasons may include the following two aspects. First, the stiffness of the joint driving rod is approximately 30 N/mm. When the finger is closed for 2 mm, the applied force is approximately 60 N. This is well below the force that can be provided by the lead screw. Second, the finger is relative thin and the arrangement of the finger linkage is not optimized for force magnification. Nonetheless, this paper primarily demonstrates the features and application of the CCM.

With the current design, the CoMPS can still be used as a training device for synergy control. However, the force capability may limit its use as prosthesis or in a humanoid service robot.

6.4. Pull-out experiments

The pull-out experiments were performed as shown in Fig. 10(c). A baseball was grasped and then pulled out. The pull-out motion was realized by a lead screw and the pull-out force was measured using a force gauge (HF-50 from Zhengkai Precision Instrument Co., China) with a built-in function for peak force measurement and a measurement range of ± 50 N.

The pull-out forces are plotted in Fig. 10(c), where the finger-closing actuation increases from 0.6 mm to 2 mm. The plot displays the minimal, the average and the maximal forces of the pull-out experiments, which were repeated five times.

The results from the pull-out experiments indicate the capability of the CoMPS hand in maintaining a grasp under a directed external disturbance. The baseball was pulled out by prying the fingers open. It can be seen from Fig. 10(c) that the pull-out force proportionally increases with respect to the finger closing length. The results are consistent with the expectation that closing the fingers harder generates a bigger pull-out force. The pull-out force will be substantially bigger under the same finger closing actuation, if the pull-out motions can be blocked by the hand's structures.

7. Conclusions

Continuum mechanisms, in addition to their widely known uses as manipulator bodies and catheter tips, can be alternatively used as transmission units. Along with the recently introduced continuum differential mechanisms, this paper proposes a Composed Continuum Mechanism that can generate an arbitrary number of translational outputs by linearly combining two independent inputs.

Features of the proposed CCM were demonstrated as the mechanical postural synergies of the constructed CoMPS hand. In the coordinated motion mode, three actuators drive the CCM to generate eleven outputs to drive the hand joints to form synergy-based hand poses in a pre-grasp phase. Then, the actuators drive the CCM to close the fingers in a synchronized motion mode. Joint-level compliance was selectively introduced based on a statics analysis to help achieve stable grasps and pinches of many daily life objects.

Please cite this article as: K. Xu et al., Composed continuum mechanism for compliant mechanical postural synergy: An anthropomorphic hand design example, Mechanism and Machine Theory (2018), https://doi.org/10.1016/j.mechmachtheory.2018.08.015

The model-based compliance calculation, postural synergy synthesis, system descriptions and experimentation of this CoMPS hand are elaborated. The hand poses used for the synergy synthesis can be mostly reproduced, although some poses involved noticeable joint errors on the non-contacting fingers. Stable grasps and pinches were realized.

The CoMPS hand can be used as a training device. An amputee can learn how to drive the synergy-based hand to form hand poses in the pre-grasp phase, and then close the fingers to produce stable grasps and pinches. The presented sensitivity studies indicate how accurate an amputee shall reproduce the pre-grasp poses, providing a clear learning goal.

With the finger linkages optimized and the grasping forces increased, the CoMPS hand can be used in a humanoid service robot. Using customized lead screw motors and a shortened CCM to reduce the length of the CoMPS hand can enable its use as a prosthetic hand.

It is the hope that the presented CoMPS hand can inspire more designs using the CCM for generating outputs that are linearly combined from two inputs, particularly when many outputs are required within a limited design volume where the CCM's structural simplicity and efficacy is advantageous.

Acknowledgments

This work was supported in part by the National Natural Science Foundation of China (Grant No. 51722507, Grant No. 51435010 and Grant No. 91648103), and in part by the National Key R&D Program of China (Grant No. 2017YFC0110800).

Supplementary materials

Supplementary material associated with this article can be found, in the online version, at doi:10.1016/j.mechmachtheory.2018.08.015.

References

[1] G. Robinson, J.B. Davies, Continuum robots–a state of the art, in: Proceedings of the IEEE International Conference on Robotics and Automation (ICRA), Detroit, Michigan, 1999, pp. 2849–2853.
[2] R.J. Webster, B.A. Jones, Design and kinematic modeling of constant curvature continuum robots, Rev. Int. J. Robot. Res. 29 (2010) 1661–1683.
[3] N. Simaan, K. Xu, A. Kapoor, W. Wei, P. Kazanzides, P. Flint, R.H. Taylor, Design and integration of a telerobotic system for minimally invasive surgery of the throat, Int. J. Robot. Res. 28 (2009) 1134–1153.
[4] J. Ding, R.E. Goldman, K. Xu, P.K. Allen, D.L. Fowler, N. Simaan, Design and coordination kinematics of an insertable robotic effectors platform for single-port access surgery, IEEE/ASME Trans. Mechatron. 18 (2013) 1612–1624.
[5] K. Xu, J. Zhao, M. Fu, Development of the SJTU Unfoldable Robotic System (SURS) for single port laparoscopy, IEEE/ASME Trans. Mechatron. 20 (2015) 2133–2145.
[6] J. Burgner-Kahrs, D.C. Rucker, H. Choset, Continuum Robots for medical applications: a survey, IEEE Trans. Robot. 31 (2015) 1261–1280.
[7] N. Bernstein, The problem of the interrelation of coordination and localization, Arch. Biol. Sci. 38 (1935) 1–34.
[8] M. Santello, M. Flanders, J.F. Soechting, Postural hand synergies for tool use, J. Neurosci. 18 (1998) 10105–10115.
[9] M.T. Ciocarlie, C. Goldfeder, P.K. Allen, Dexterous grasping via eigengrasps: a low-dimensional approach to a high-complexity problem, Robot. Sci. Syst. (2007).
[10] M.R. Cutkosky, On grasp choice, grasp models, and the design of hands for manufacturing tasks, IEEE Trans. Robot. Autom. 5 (1989) 269–279.
[11] T. Feix, R. Pawlik, H.-B. Schmiedmayer, J. Romero, D. Kragić, A comprehensive grasp taxonomy, in: Proceedings of the Robotics, Science and Systems Conference (RSS), Seattle, Washington USA, 2009.
[12] J.Z. Zheng, S. De La Rosa, A.M. Dollar, An investigation of grasp type and frequency in daily household and machine shop tasks, in: Proceedings of the IEEE International Conference on Robotics and Automation (ICRA), Shanghai, China, 2011, pp. 4169–4175.
[13] M.T. Ciocarlie, P.K. Allen, Hand posture subspaces for dexterous robotic grasping, Int. J. Robot. Res. 28 (2009) 851–867.
[14] A. Bicchi, M. Gabiccini, M. Santello, Modelling natural and artificial hands with synergies, Philos. Trans. R. Soc. B Biol. Sci. 366 (2011) 3153–3161.
[15] J. Rosell, R. Suárez, C. Rosales, A. Pérez, Autonomous motion planning of a hand-arm robotic system based on captured human-like hand postures, Auton. Robots 31 (2011) 87–102.
[16] M. Gabiccini, E. Farnioli, A. Bicchi, Grasp analysis tools for synergistic underactuated robotic hands, Int. J. Robot. Res. 32 (2013) 1553–1576.
[17] D. Prattichizzo, M. Malvezzi, M. Gabiccini, A. Bicchi, On motion and force controllability of precision grasps with hands actuated by soft synergies, IEEE Trans. Robot. 29 (2013) 1440–1456.
[18] K. Xu, H. Liu, Y. Du, X. Zhu, Design of an underactuated anthropomorphic hand with mechanically implemented postural synergies, Adv. Robot. 28 (2014) 1459–1474.
[19] M.G. Catalano, G. Grioli, E. Farnioli, A. Serio, C. Piazza, A. Bicchi, Adaptive synergies for the design and control of the Pisa/IIT SoftHand, Int. J. Robot. Res. 33 (2014) 768–782.
[20] T. Wimböck, B. Jahn, G. Hirzinger, Synergy level impedance control for multifingered hands, in: Proceedings of the IEEE/RSJ International Conference on Intelligent Robots and Systems (IROS), San Francisco, CA, USA, 2011, pp. 973–979.
[21] F. Ficuciello, G. Palli, C. Melchiorri, B. Siciliano, Experimental evaluation of postural synergies during reach to grasp with the UB hand IV, in: Proceedings of the IEEE/RSJ International Conference on Intelligent Robots and Systems (IROS), San Francisco, CA, USA, 2011, pp. 1775–1780.
[22] E. Rombokas, M. Malhotra, Y. Matsuoka, Task-specific Demonstration and Practiced Synergies for Writing with the ACT Hand, in: Proceedings of the IEEE International Conference on Robotics and Automation (ICRA), Shanghai, China, 2011, pp. 5363–5368.
[23] A. Zhang, M. Malhotra, Y. Matsuoka, Musical Piano Performance by the ACT Hand, in: Proceedings of the IEEE International Conference on Robotics and Automation (ICRA), Shanghai, China, 2011, pp. 3536–3541.
[24] G. Palli, C. Melchiorri, G. Vassura, U. Scarcia, L. Moriello, G. Berselli, A. Cavallo, G.D. Maria, C. Natale, S. Pirozzi, C. May, F. Ficuciello, B. Siciliano, The DEXMART hand: mechatronic design and experimental evaluation of synergy-based control for human-like grasping, Int. J. Robot. Res. 33 (2014) 799–824.
[25] C.Y. Brown, H.H. Asada, Inter-finger coordination and postural synergies in robot hands via mechanical implementation of principal components analysis, in: Proceedings of the IEEE/RSJ International Conference on Intelligent Robots and Systems (IROS), San Diego, CAU, SA, 2007, pp. 2877–2882.
[26] S. Li, X. Sheng, H. Liu, X. Zhu, Design of a myoelectric prosthetic hand implementing postural synergy mechanically, Ind. Robot Int. J. 41 (2014) 447–455.
[27] W. Chen, C. Xiong, S. Yue, Mechanical implementation of kinematic synergy for continual grasping generation of anthropomorphic hand, IEEE/ASME Trans. Mechatron. 20 (2015) 1249–1263.

Please cite this article as: K. Xu et al., Composed continuum mechanism for compliant mechanical postural synergy: An anthropomorphic hand design example, Mechanism and Machine Theory (2018), https://doi.org/10.1016/j.mechmachtheory.2018.08.015

[28] C.-H. Xiong, W.-R. Chen, B.-Y. Sun, M.-J. Liu, S.-G. Yue, W.-B. Chen, Design and implementation of an anthropomorphic hand for replicating human grasping functions, IEEE Trans. Robot. 32 (2016) 652–671.
[29] K. Xu, H. Liu, Y. Du, X. Sheng, X. Zhu, Mechanical implementation of postural synergies using a simple continuum mechanism, in: Proceedings of the IEEE International Conference on Robotics and Automation (ICRA), Hong Kong, China, 2014, pp. 1348–1353.
[30] G.C. Matrone, C. Cipriani, E.L. Secco, G. Magenes, M.C. Carrozza, Principal components analysis based control of a multi-dof underactuated prosthetic hand, J. Neuroeng. Rehab. 7 (2010) 16–28.
[31] K. Xu, H. Liu, Continuum differential mechanisms and their applications in gripper designs, IEEE Trans. Robot. 32 (2016) 754–762.
[32] G.C. Matrone, C. Cipriani, M.C. Carrozza, G. Magenes, Two-channel real-time emg control of a dexterous hand prosthesis, in: Proceedings of the International IEEE/EMBS Conference on Neural Engineering (NER), Cancun, Mexico, 2011, pp. 554–557.
[33] J.L. Segil, R.F.F Weir, Design and validation of a morphing myoelectric hand posture controller based on principal component analysis of human grasping, IEEE Trans. Neural Syst. Rehab. Eng. 22 (2014) 249–257.
[34] B. Alexander, K. Viktor, Proportions of hand segments, Int. J. Morphol. 28 (2010) 755–758.
[35] R. Hamilton, R.A. Dunsmuir, Radiographic assessment of the relative lengths of the bones of the fingers of the human hand, J. Hand Surg. 27 (2002) 546–548.
[36] J.T. Belter, J.L. Segil, A.M. Dollar, R.F. Weir, Mechanical design and performance specifications of anthropomorphic prosthetic hands: a review, J. Rehab. Res. Develop. 50 (2013) 599–618.
[37] G. Gioioso, G. Salvietti, M. Malvezzi, D. Prattichizzo, Mapping synergies from human to robotic hands with dissimilar kinematics: an approach in the object domain, IEEE Trans. Robot. 29 (2013) 825–837.
[38] K. Xu, N. Simaan, An investigation of the intrinsic force sensing capabilities of continuum robots, IEEE Trans. Robot. 24 (2008) 576–587.
[39] K. Xu, N. Simaan, Analytic formulation for the kinematics, statics and shape restoration of multibackbone continuum robots via elliptic integrals, J. Mech. Robot. 2 (2010) 1–13.
[40] G. Carbone, Grasping in Robotics, Springer-Verlag, London, 2013.

Please cite this article as: K. Xu et al., Composed continuum mechanism for compliant mechanical postural synergy: An anthropomorphic hand design example, Mechanism and Machine Theory (2018), https://doi.org/10.1016/j.mechmachtheory.2018.08.015